Journal of Physics D: Applied Physics

PAPER • OPEN ACCESS

TiO_2 multi-leg nanotubes for surface-enhanced Raman scattering

To cite this article: Harini S *et al* 2024 *J. Phys. D: Appl. Phys.* **57** 325106

OPEN ACCESS
IOP Publishing
Journal of Physics D: Applied Physics
J. Phys. D: Appl. Phys. **57** (2024) 325106 (9pp)
https://doi.org/10.1088/1361-6463/ad42a9

TiO_2 multi-leg nanotubes for surface-enhanced Raman scattering

Harini S[1], Garima Gupta[2], Somnath C Roy[2] and Rambabu Yalavarthi[1,3,*]

[1] Department of Physics, School of Advanced Sciences, Vellore Institute of Technology Vellore, Tiruvalam road, Katpadi 632014, Tamilnadu, India
[2] Semiconducting Oxide Materials, Nanostructures and Tailored Heterojunctions (SOMNaTH) Lab, Department of Physics, Indian Institute of Technology Madras, Chennai 600036, Tamilnadu, India

E-mail: rambabu.y@vit.ac.in and r.yalavarthi@physik.uni-muenchen.de

Received 1 December 2023, revised 5 March 2024
Accepted for publication 24 April 2024
Published 21 May 2024

Abstract

In the recent past, significant research efforts have been put forth to fabricate cost-effective substrates for surface-enhanced Raman scattering (SERS) applications. Here we propose semiconducting TiO_2 multi-leg nanotubes and Au nanoparticle-coated TiO_2 multi-leg nanotubes (TiO_2 MLNTs and Au/TiO_2 MLNTs) as SERS substrates. The unique multi-leg architecture of TiO_2 nanotubes demonstrated enhanced light-harvesting properties facilitated by an induced photonic absorption edge. Remarkable high SERS sensitivity is observed towards the detection of Methylene blue (MB), up to nM concentration (E.F. $\sim 10^4$) using TiO_2 MLNTs. The same is attributed to the resonantly matched photonic absorption edge of TiO_2 MLNTs with the wavelength of incident laser probe light. On the other hand, the Au nanoparticle coating further leveraged the light absorption ability of TiO_2 MLNTs with the aid of localized surface plasmon resonance mode. As such, Au/TiO_2 MLNTs showed excellent enhancement in SERS sensitivity (E.F. $\sim 10^5$, for nM of MB) facilitated by the synergy between the plasmonic modes of Au and the photonic absorption mode of TiO_2 MLNTs. UV-Vis diffuse reflectance and Raman spectroscopy measurements are highlighted to elucidate the light absorption and SERS sensitivity of the TiO_2 and Au/TiO_2 MLNTs.

Supplementary material for this article is available online

Keywords: TiO_2 nanotubes, metasurfaces, metal nanostructure, SERS, light absorption, plasmonics

1. Introduction

Surface-enhanced Raman scattering (SERS) is a powerful non-destructive technique that allows highly sensitive detection of trace amounts of chemical and biological analytes [1, 2]. SERS has found its applications in material sciences [3], chemical analysis [4], biomedical research [5], forensics [6], etc. Recent developments have led to molecular imaging [7], photo-electrochemical characterizations [8, 9], and even single-molecule detection [10, 11].

SERS relies on the interaction between incident light and the nanostructured substrates of noble metals, for example, Au, and Ag [1]. The SERS sensitivity of molecules adsorbed on a noble metal substrate is attributed to the electromagnetic (EM) enhancement associated with a charge transfer process (chemical enhancement) at the EM 'hot spots' [12]. EM enhancement is proportional to the electric field (hot

[3] Present address: Nanoinstitute Munich, Faculty of Physics, Ludwig-Maximilians-Universität München, München 80539, Germany.
[*] Author to whom any correspondence should be addressed.

spots) generated by the resonantly excited free electrons of the metal surface upon the interaction with light [1]. In the vicinity of these hot spots, the plasmon-induced near fields effectively couple to the vibrational modes of adsorbed molecules and thus amplify the Raman signal cross-section several times [13]. The magnitude of the electric field intensity depends on the size, shape, gap, and composition of the metal nanostructure [9, 14, 15]. Therefore, to achieve better SERS sensitivity with higher enhancements in a reproducible manner, it is indeed necessary to fabricate the tailored nanostructures of metals [13, 16]. However, due to the high cost, low abundance, biocompatibility, and re-usability, the use of noble metals is limited in the fabrication process of SERS substrates [13].

In this context, semiconductor nanostructures have been proposed to minimize the metal content in the fabrication of SERS substrates [17–19]. These nanostructures either themselves act as SERS substrates or provide structural support for the anchoring of noble metals [17, 20, 21]. As such, the metal content can be minimized significantly. The SERS intensity of pristine semiconductors (e.g. TiO_2, ZnO) is generally attributed to the enhanced light-matter interaction facilitated by the photonic band gap [17, 20–22]. Qi *et al* reported noble metal-free TiO_2 photonic microarray SERS substrates. The SERS activity of such photonic band nanostructured substrates (PBNs) is mainly attributed to the resonantly matched photonic absorption edge with the incident wavelength of laser probe light [17]. Thus, the main criterion for SERS enhancement in PBNs is the tuning of the photonic absorption edge in correlation with the wavelength of incident laser probe light [21]. The photonic band edge in semiconductors can be altered by modifying the nanostructure's shape, size, and periodicity [23]. However, the enhancement factors of PBNs are generally low when compared to the noble metal SERS substrates [17]. To address this problem, a strategy for making photonic-plasmonic nanocomposites (noble metal nanostructure anchored PBNs) has been proposed. The localized surface plasmon resonance mode (LSPRs) associated with the noble metal nanostructures synergistically couple to the photonic band edge and thus greatly enhance the SERS intensity. Till now, only a few studies focused on the fabrication of SERS substrates of LSPRs-coupled PBNs. For example, Franz *et al* reported Au nanoparticle decorated porous silica photonic substrates for enhanced SERS [20]. In another report by Wang *et al*, photonic-plasmonic microspheres composed of SiO_2 nanospheres decorated with gold nanoparticles have been studied for enhanced SERS [21]. Mu *et al* explored the Au nanocrystal-incorporated bio-inspired photonic structures [24]. Ben-Jaber *et al* designed several Au-semiconductor systems for studying with photo-induced SERS the oxygen vacancies dynamics and their impact on photocatalysis [25–27]. However, the fabrication procedures of such tailored nanostructures are complex and require expensive equipment, e.g. lithography. Other fabrication procedures such as template-assisted methods and self-assembly of nanoparticles over solid surfaces are time-consuming and it is difficult to scale up into large dimensions [28, 29].

Here, for the first time, we show TiO_2 multi-leg nanotubes (TiO_2 MLNTs) as well as gold nanoparticle-coated TiO_2 MLNTs (Au/TiO_2 MLNTs) as potential SERS substrates. The method of fabrication process of these substrates is simple and achieved via single-step electrochemical anodization, followed by an Au layer (thickness, 10–30 nm) sputtered over the nanotubes and subsequent annealing in air ambient [30, 31]. Moreover, the unique multi-leg morphology resembles the gradient refractive index layered architecture, and thus TiO_2 MLNTs demonstrate excellent light harvesting ability in comparison to the other compact nanotubes [30]. As such, the tubes can act as PBNs as discussed above [20, 22, 23]. In addition, due to the spacing between tube to tube, it is very easy to form a composite nanostructure with a suitable other light absorption material without destroying the morphology of nanotube architecture [32]. Thus the TiO_2 MLNTs not only provide the required support structure for the anchoring Au nanoparticles but also resemble PBNs to couple the LSPRs associated with the Au [14, 33]. As such, the fabricated substrates demonstrated excellent SERS activity towards the detection of Methylene blue (MB). A SERS enhancement factor (E.F.) of about $\sim 2.5 \pm 1.1 \times 10^4$ is measured for bare TiO_2 MLNTs for nM MB concentration. This is attributed to the enhanced light-matter interaction facilitated by the photonic band (PBN) [30]. Further improvement in SERS sensitivity with an E.F. of $\sim 9.7 \pm 1.5 \times 10^4$ is recorded for Au/TiO_2 MLNTs (Au-60 s; MB-nM), which is approximately one order higher E.F. compared to that of bare MLNTs. The enhancement is attributed to the synergy that exists between photonic and plasmonic bands. We discuss the role of multi-leg morphology towards the detection of MB (SERS; up to nM concentration) as well as the synergy that exists between photonic and plasmonic modes of Au/TiO_2 MLNTs and their influence in enhancing the SERS sensitivity in connection with the light absorption spectra.

2. Experimental section

2.1. Fabrication of TiO_2 MLNTs

TiO_2 MLNTs were synthesized by the electrochemical anodization method as per the protocol described in previous reports [30, 31]. Briefly, Titanium foil (20 mm × 20 mm × 0.25 mm; 99.7% purity, Sigma-Aldrich) was used as an anode, and a Pt foil of a similar dimension was used as a cathode. Initially, Ti foils were cleaned in de-ionized water, ethanol, and acetone for 5 min each with an ultrasonic cleaner, and dried in ambient air. A mixture of 96 ml di-ethylene glycol, Merck, 4 ml of de-ionized water, and 0.6 wt% of ammonium bi-fluoride salt (NH_4HF_2, Merck) was stirred in a 100 ml beaker using a magnetic stirrer for 30 min and used as the electrolyte solution. The anodization was carried out for 2 h with a constant voltage of 60 V at room temperature of about 30 °C. It has been attributed that, higher voltage (~60 V) and existence of two fluoride ions in the electrolyte (NH_4^+ and H^+) are the factors that influence the growth of multi-leg morphology. The hydrodynamic radii can influence the diffusion coefficient and mobility of fluoride ions in the electrolyte. Therefore, higher hydrodynamic radii

and greater mobility of NH_4^+ ions in comparison to the H^+ can lead to the gradient in the viscosity of the electrolyte. Thus two or more tubes at the top fuse together to form multi-leg morphology [30]. After anodization, the samples were rinsed thoroughly with isopropyl alcohol and de-ionized water and kept at room temperature for 1 h to dry.

2.2. Fabrication of gold nanoparticle-coated TiO_2 MLNTs

Subsequently, a thin film of gold was deposited on the as-obtained TiO_2 MLNTs by sputtering technique. EMS 150 R ES sputter coater system was used to deposit the thin film of gold with an applied current of 20 mA at room temperature and at a pressure of Ar, 8×10^{-2} mBar. The deposition was carried out for a period of 30–90 s to vary the thickness of the gold film. Eventually, the gold layer-coated TiO_2 MLNTs were annealed at 450 °C in a tubular furnace for 2 h with the ramp setting of 1 °C min^{-1}. During the process of annealing, the gold film deposited over TiO_2 nanotubes turned into gold nanoparticles due to the de-wetting phenomenon and as a result, Au nanoparticle-coated TiO_2 MLNTs (Au/TiO_2 MLNTs) were formed. A probe analyte, MB was used to investigate the SERS enhancement. Initially, MB was deposited by immersing different substrates (Bare TiO_2, and 30 s, 60 s and 90 s Au deposited TiO_2 MLNTs) in 20 ml of varying molar concentrations of MB (nM to mM) for 24 h.

2.3. Characterization

X-ray diffraction (XRD) analysis was executed in a 2θ range of 20°–60° by Bruker D8 Advance x-ray diffractometer equipped with a 2.2 KW Cu Kα anode source. A scanning electron microscope (SEM, FEI Inspect 550) was used to analyze the surface morphology, and Image-J software was used to analyze the size of nanostructures. Similarly, energy dispersive spectroscopy (EDS) measurements were performed to determine the elemental composition of the samples. UV-Vis diffuse reflectance measurements (DRS) were performed using Perkin Elmer Lambda 950 spectrophotometer equipped with an integrating sphere. Raman measurements were performed using a Renishaw Raman microscope to analyze the SERS enhancement. All spectra were recorded in the range 700–2000 cm^{-1} with an acquisition time of 10 s and measured on at least three different spots of the sample. The laser power (2 mW) and beam spot are kept constant throughout all measurements. Origin software was used for baseline correction and peak analysis.

3. Results and discussion

3.1. Morphology and structural characterization

Figures 1 and S1 (supplementary information) show the FE-SEM images of bare and Au nanoparticle-coated TiO_2 MLNTs. Figure 1(a) demonstrates the branched morphology of a multi-leg nanotube structure with the combination of three or more tubes fused at the top, with a pore diameter ranging between 120 ± 5 nm to 330 ± 6 nm, and the average diameter is ∼200 nm. Such a multi-leg morphology offers a change in effective refractive index (n_{eff}) from top to bottom [30]. The gradient in n_{eff} along the tube length allows the light to scatter multiple times within the MLNTs, thus significantly enhancing the light-matter interaction (figure S2, supplementary information). As such, TiO_2 MLNTs resemble the PBNs with a photonic absorption edge. The surface morphology of Au deposited (for 30 s, 60 s, and 90 s) TiO_2 MLNTs by sputtering technique followed by annealing have been presented in figures 1(b)–(d) and S3(a)–(c), (supplementary information) respectively. The morphological observations reveal that the spherical Au nanoparticles are distributed homogenously on the top and side walls of the nanotubes. The size of Au nanoparticles varies from 10 ± 2 nm to 45 ± 3 nm with the change in deposition time from 30 to 90 s.

XRD patterns shown in figure 2(a) demonstrate the phase composition and crystal structure of TiO_2 and Au/TiO_2 MLNTs. The characteristic peak at a 2θ value of 25.28° corresponding to the (110) plane indicates the anatase crystal phase of TiO_2 in both samples (JCPDS: 87-0920) [31]. In addition, the predominant peaks appeared at 2θ values of 35.24°, 38.58°, 40.30°, and 53.11° correspond to (100), (002), (101), and (102) crystal planes represent the Titanium substrate (JCPDS: 89-2762). XRD peak corresponding to metallic Au nanoparticles at a 2θ value of 38.10° is overlapped with the peak corresponding to the Titanium at the same position [14]. This can be understood by observing the difference in intensities of the peak that appeared at 38.1° for TiO_2 and Au/TiO_2 MLNTs.

Raman measurements are also considered to characterize the crystal structure and phase of the prepared samples. Figure 2(b) shows the Raman spectra of TiO_2 and Au/TiO_2 MLNTs. The spectra confirm the anatase phase of TiO_2 MLNTs with the Raman vibrational modes corresponding to $E_{g(1)}$ at 145 cm^{-1}, $E_{g(2)}$ at 199 cm^{-1}, B_{1g} at 395 cm^{-1}, $A_{1g} + B_{1g}$ at 513 $cm^{-1,}$ and $E_{g(3)}$ at 637 cm^{-1} [31]. Further, a small blue shift in peak position at 145 cm^{-1} for Au/TiO_2 MLNTs in comparison to the bare TiO_2 MLNTs indicates the composite formation with Au nanoparticles. Figure 2(c), EDS spectra shows the elemental composition of 90 s Au sputtered TiO_2 MLNTs. The percentage (Wt%) of elements, Titanium (Ti) is about 59.4%, oxygen (O) is 36.2% and Au is 4.4%, which reveals the reduced content of expensive noble metals (Au) in the fabrication process of SERS substrates.

3.2. Light absorption properties

Figure 3(a) shows the absorbance spectra (1-R) of TiO_2 MLNTs with and without the Au nanoparticles obtained from the DRS measurements. The absorption edge at ∼390 nm represents the electronic band gap of bare TiO_2 MLNTs, which is ∼3.16 eV. In addition, the spectra also show broad absorption corresponding to the wavelength range 400–700 nm. Defects (oxygen vacancies) could be the reason for such an absorption. However, previous studies ruled out the possible existence of defects in TiO_2 MLNTs [34]. On the other hand, it has been

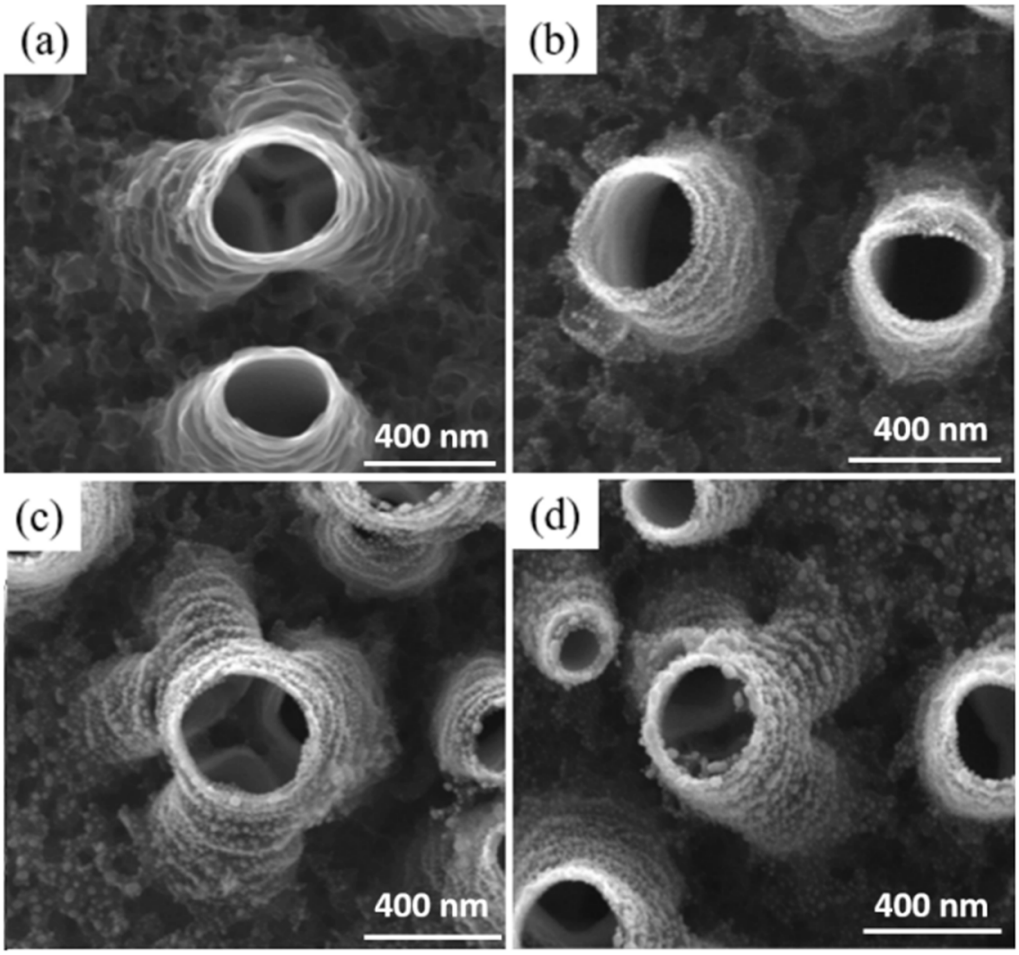

Figure 1. FE-SEM images of bare and Au nanoparticle-coated TiO_2 MLNTs. (a) bare TiO_2 MLNTs. (b) Au/TiO_2 MLNTs; Au-30 s. (c) Au/TiO_2 MLNTs; Au-60 s. (d) Au/TiO_2 MLNTs; Au-90 s.

shown that the coefficient of specular reflection (R) reduced by a factor of 102 in comparison to the non-multi-leg tubes due to the change in n_{eff} (top section-1.06; middle section-1.14; and bottom section-2.49 of lengths 1.2, 1.6 and 0.2 μm respectively) along the tube length [30]. Therefore, we attribute such a broad absorption to the characteristic gradient refractive index profile of TiO_2 MLNTs facilitated by the multiple reflections of incident light from the Ti substrate [30]. As such, the gradient in n_{eff} slows down the velocity of incident light within the layered morphology and generates a photonic absorption edge peaking at 535 nm and thus significantly enhances the light-matter interaction [17, 22]. Similarly, a sharp peak at ~535–550 nm is measured for Au/TiO_2 MLNTs (Au-30–90 s). A linear increment in intensity and a red shift in peak position is observed with the change in Au deposition time, which we attributed to the variation in Au nanoparticle size upon an increase in deposition time. To better understand, we have de-convoluted the peak using Lorentzian fitting and spectra are shown in figure 3(b). The fitting peak of wavelength range 440–475 nm corresponding to the energy 2.6–2.8 eV, is attributed to the characteristic inter-band, *d-sp* transitions of Au, and is thus responsible for the LSPRs associated with the Au nanoparticles [14, 16]. In general, for pristine Au nanostructures, the intense local electric fields corresponding to LSPRs generate so-called *'hot spots'* in the vicinity of the probe molecules and thus enhance the Raman absorption cross-section by many folds [14, 16]. However, apart from the LSPR peak, there is another fitting peak in the range 535–550 nm corresponding to the energy ~2.5–2.3 eV. This is in line with the photonic absorption edge (~535) nm of TiO_2 MLNTs as discussed above. Therefore, the coupling between the photonic mode and LSPR peak generates a new hybrid cavity mode, which is the absorption peak observed for Au/TiO_2 MLNTs and is thus responsible for the SERS enhancement.

3.3. SERS characterization studies

Raman measurements were performed to examine the SERS sensitivity of the TiO_2 and Au/TiO_2 MLNTs using a probe analyte MB and are shown in figure 4. Three molar concentrations (mM, μM, and nM) of MB were considered to analyze the SERS enhancement. Numerous peaks at frequencies 875, 950, 1035, 1183, 1301, 1393, 1445, and 1625 cm^{-1} are observed for the SERS spectra of MB [35]. All these peaks represent the

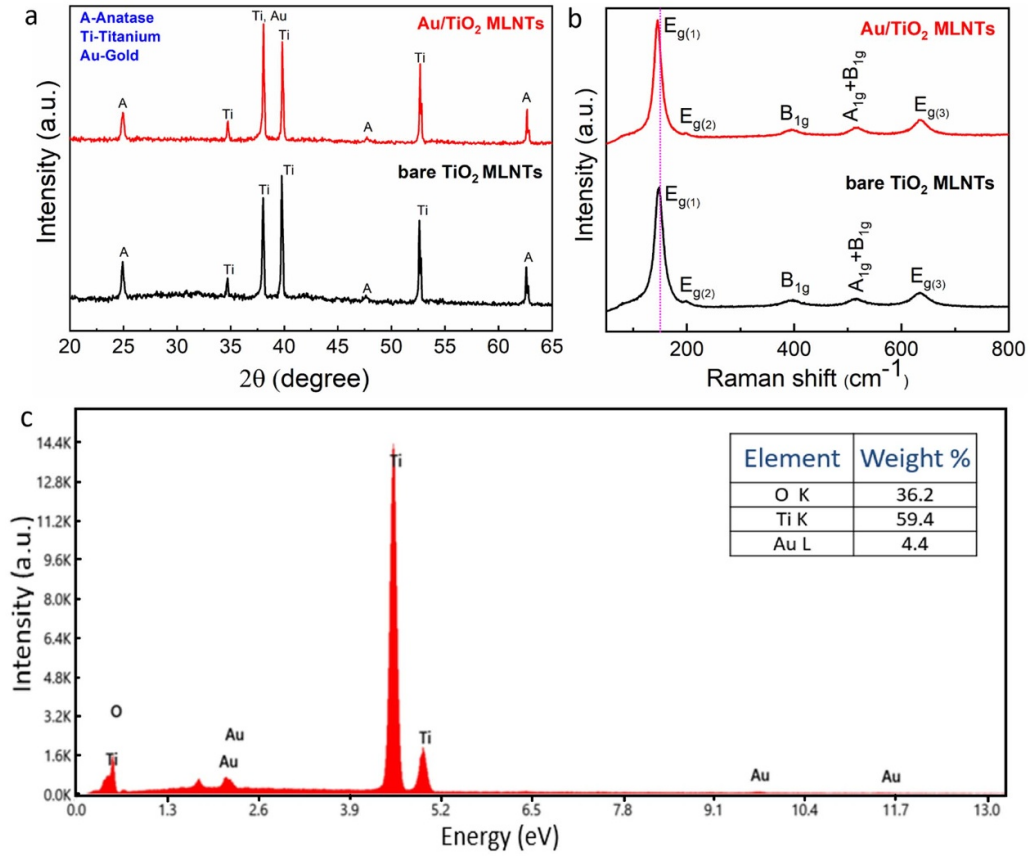

Figure 2. (a) XRD patterns of TiO_2 MLNTs with and without the Au nanoparticles (Au-60 s). (b) Raman spectra of TiO_2 MLNTs with and without the Au nanoparticles (Au-60 s). (c) EDS spectrum of Au /TiO_2 MLNTs (Au-90 s).

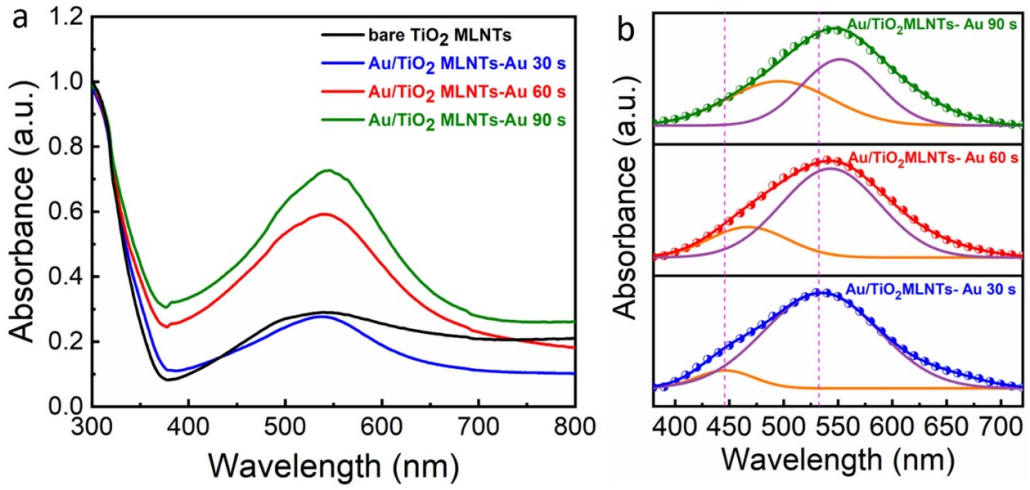

Figure 3. (a) DRS spectra (absorbance) of TiO_2 and Au/TiO_2 MLNTs. (b) Lorentzian fitting of absorption peak (400–700 nm), corresponding to Au/TiO_2 MLNTs.

various vibrational modes of MB, and comprehensive details of these vibrational modes can be found in the literature [35]. The prominent peak that appeared at 1625 cm^{-1} is assigned to the v(C–C)/v(C–N) mixed stretching mode of MB, which was chosen to compare the SERS enhancement among all samples by varying the concentration of MB (nM to mM). Figure 4(a) demonstrates the SERS sensitivity of bare TiO_2 MLNTs in comparison with a non-SERS spectrum. Interestingly, bare TiO_2 MLNTs themselves showed significant enhancement in SERS activity for the detection of MB up to nM concentrations. Here, the SERS activity of bare TiO_2 MLNTs is mainly attributed to the enhanced light-matter interaction. Bare TiO_2

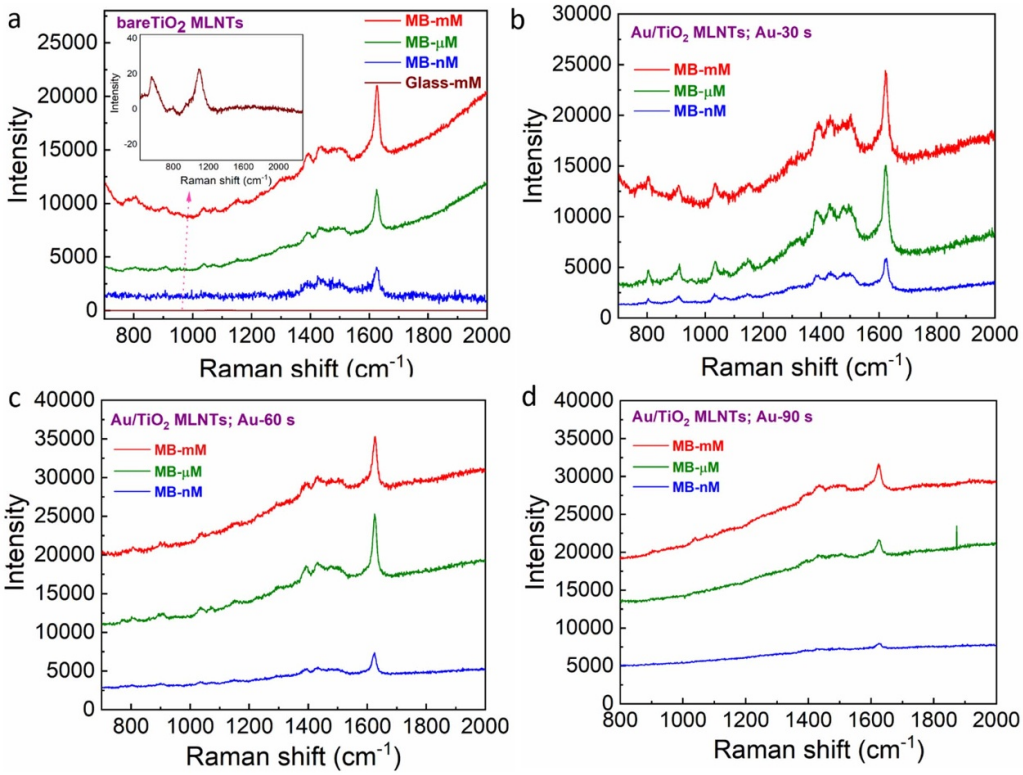

Figure 4. (a) SERS spectra of bare TiO_2 MLNTs (mM, μM, and nM), and glass substrate modified with mM concentrations of MB. (b) SERS spectra of Au/TiO_2 MLNTs modified with mM, μM, and nM concentrations of MB; Au-30 s. (c) SERS spectra of Au/TiO_2 MLNTs modified with mM, μM, and nM concentrations of MB; Au-60 s. (d) SERS spectra of Au/TiO_2 MLNTs modified with mM, μM, and nM concentrations of MB; Au-90 s.

MLNTs displayed a broad absorption peak at ∼535 nm, which is the photonic absorption edge of TiO_2 MLNTs. Here, it should be noted that the incident wavelength of the laser probe light is 532 nm. Therefore, during the SERS measurements, the incident laser light resonantly couples with the existing photonic absorption edge of TiO_2 MLNTs. Thus enhances the light-matter interaction significantly in the vicinity of the probe molecule adsorbed on TiO_2 MLNTs. As a result, the Raman signal of the probe molecule is enhanced several times, the same is displayed in figure 4(a). Therefore, we emphasize that the gradient refractive index profile associated with TiO_2 MLNTs played a crucial role in promoting the multiple reflections of light as well as generating the photonic stop bands for the enhanced light matter-coupling.

Similarly, the measured SERS spectra for different sputter deposition times of Au thin film (30–90 s) are displayed in figures 4(b)–(d). As expected, the spectra reveal a further increase in the intensity of the MB Raman signal. For a better comparison, the baseline-corrected SERS spectra of bare and Au/TiO_2 MLNTs are presented in figure 5(a) for the mM concentration of MB. The intensity of the peak appeared at 1625 cm^{-1} following the trend of Au deposition times (30 s–60 s), whereas the peak intensity is slightly decreased for 90 s deposition. Such an enhancement in the SERS signal is attributable to the combined role of photonic modes and plasmonic modes (hybrid cavity mode) associated with the Au/TiO_2 MLNTs. Similarly, the same hybrid cavity mode is also attributed to the decrease in intensity of the SERS signal for Au/TiO_2 MLNTs (Au, 90 s). As shown in figure 3(b), the intensity of the plasmonic mode follows the trend of Au deposition time, whereas the photonic mode intensity follows the reverse trend with the increase in Au deposition time. Therefore, the splitting between photonic and plasmonic bands determines the energy of the hybrid cavity mode and thus eventually determines the ability to enhance the SERS sensitivity for a particular sample. As such, the synergy that exists between the LSPR modes coupled with the photonic modes of TiO_2 MLNTs plays a crucial role in multiplying the light-matter interaction [33]. Here, it is worth mentioning that, the above analogy is a qualitative description; however, the same complementation among photonic and plasmonic modes associated with the metal and/or semiconductor nanostructures is also been reported for other applications in the literature [14, 33, 36].

Since the enhancement factor (E.F.) is a significant number in assessing the sensitivity of SERS substrates, here, we estimated the E.F. of our SERS substrates using the following formula [37].

$$\text{E.F.} = \frac{I_{\text{SERS}}}{N_{\text{SERS}}} \times \frac{N_0}{I_0}$$

where I_{SERS} and I_o are the intensities of the SERS signal observed at 1625 cm^{-1} for bare TiO_2 MLNTs, Au/TiO_2

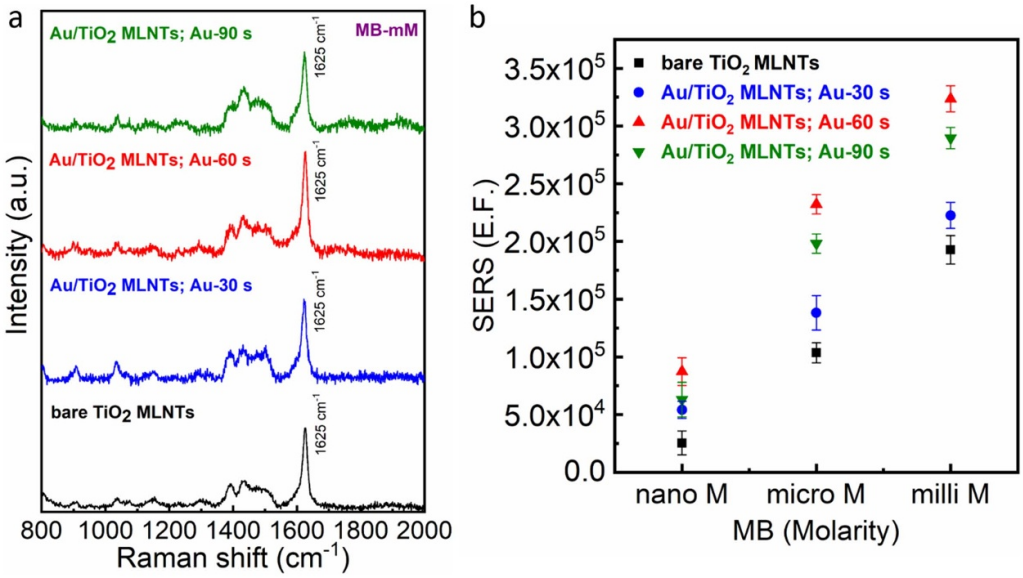

Figure 5. (a) Baseline corrected SERS spectra of TiO_2 and Au/TiO_2 MLNTs (MB-mM). (b) Enhancement factor trend of all prepared samples for all molar concentrations of MB.

MLNTs, and a non-SERS substrate (glass slide). N_{SERS} and N_o are the number of probe molecules contributing to the SERS signal (TiO_2 or Au/TiO_2 MLNTs) and the non-SERS signal (glass substrate).

Since, we used similar MB deposition and SERS activity measurement (laser power, incident spot size, acquisition time, etc) conditions, the number of probe molecules is assumed to be the same for all samples (TiO_2, Au/TiO_2 MLNTs, and glass) and distributed uniformly. The E.F. of all samples for all concentrations of MB is calculated by considering the SERS intensity of the baseline corrected predominant peak that appeared at 1625 cm^{-1}. For representation purposes, baseline corrected SERS spectra of TiO_2 and Au/TiO_2 MLNTs (Au, 30–90 s) for mM concentration of MB are shown in figure 5(a). The trend of E.F. presented in figure 5(b) follows the order of Au nanoparticle deposition times 30 s and 60 s starting from the bare TiO_2 MLNTs. Whereas, for 90 s Au deposition, the SERS sensitivity slightly decreased for all molar concentrations of MB. The bare TiO_2 MLNTs showed an E.F. of $\sim 2.5 \pm 1.1 \times 10^4$ for nM and mM concentration is $\sim 1.7 \pm 1.2 \times 10^5$. This suggests the potential use of photonic semiconductor nanostructures as SERS substrates and the values are in line with the recent report on plasmon-free PBNs [17]. On the other hand, the Au/TiO_2 MLNTs (Au-60 s) has displayed the highest E.F. among all samples; for nM concentration, E.F. is $9.7 \pm 1.5 \times 10^4$, and for mM concentration, it is $3.3 \pm 1.1 \times 10^5$. These values are approximately one order higher for nM, and two times higher for mM concentrations of MB in comparison to the bare TiO_2 MLNTs. Thus, the photonic and plasmonic bands collectively acted together to enhance the SERS signal of MB. In addition, a comparison among different morphologies, fabrication methods and E.Fs has been included in table S1, supplementary information to identify the significance of the present work.

4. Conclusions

In conclusion, we demonstrate the potential use of semiconductor TiO_2 MLNTs as SERS substrates. Initially, TiO_2 MLNTs were fabricated using a simple single-step anodization method. Such nanotubes without any plasmonic support structure displayed a significant SERS sensitivity, which is attributed to the enhanced light-matter interaction facilitated by the layered structure of gradient refractive index morphology. In addition, to further improve the SERS sensitivity, we used a conformal coating of gold nanoparticles over TiO_2 MLNTs. The nanocomposite morphology (Au/TiO_2 MLNTs) exhibited enhanced SERS activity facilitated by the synergy that exists between photonic and plasmonic modes. Thus, the fabrication procedure and SERS substrates (TiO_2 MLNTs) presented in this work are simple and inexpensive and can be explored to probe analytes for physical, chemical, biological, and analytical applications.

Data availability statement

The data that support the findings of this study are available upon reasonable request from the authors.

Acknowledgments

RY acknowledges the European Commission for a Marie-Sklodowska Curie research fellowship Grant (Project-PIERCAT) and the host Professor Emiliano Cortes, Nanoinstitute Munich, University of Munich, Germany for fruitful comments and discussions.

Conflicts of interest

The authors declare no conflicts of interest.

ORCID iDs

Somnath C Roy https://orcid.org/0000-0003-4685-8742
Rambabu Yalavarthi https://orcid.org/0000-0002-5131-2843

References

[1] Itoh T, Procházka M, Dong Z-C, Ji W, Yamamoto Y S, Zhang Y and Ozaki Y 2023 Toward a new era of SERS and TERS at the nanometer scale: from fundamentals to innovative applications *Chem. Rev.* **123** 1552–634
[2] Bell S E J, Charron G, Cortés E, Kneipp J, Chapelle M L, Langer J, Procházka M, Tran V and Schlücker S 2020 Towards reliable and quantitative surface-enhanced Raman scattering (SERS): from key parameters to good analytical practice *Angew. Chem., Int. Ed.* **59** 5454–62
[3] Schedin F, Lidorikis E, Lombardo A, Kravets V G, Geim A K, Grigorenko A N, Novoselov K S and Ferrari A C 2010 Surface-enhanced Raman spectroscopy of graphene *ACS Nano* **4** 5617–26
[4] Mosier-Boss P 2017 Review of SERS substrates for chemical sensing *Nanomaterials* **7** 142
[5] Reokrungruang P, Chatnuntawech I, Dharakul T and Bamrungsap S 2019 A simple paper-based surface enhanced Raman scattering (SERS) platform and magnetic separation for cancer screening *Sens. Actuators* B **285** 462–9
[6] Muehlethaler C, Leona M and Lombardi J R 2016 Review of surface enhanced raman scattering applications in forensic science *Anal. Chem.* **88** 152–69
[7] Palonpon A F, Ando J, Yamakoshi H, Dodo K, Sodeoka M, Kawata S and Fujita K 2013 Raman and SERS microscopy for molecular imaging of live cells *Nat. Protocols* **8** 677–92
[8] Oksenberg E, Shlesinger I, Xomalis A, Baldi A, Baumberg J J, Koenderink A F and Garnett E C 2021 Energy-resolved plasmonic chemistry in individual nanoreactors *Nat. Nanotechnol.* **16** 1378–85
[9] Nan L, Giráldez-Martínez J, Stefancu A, Zhu L, Liu M, Govorov A O, Besteiro L V and Cortés E 2023 Investigating plasmonic catalysis kinetics on hot-spot engineered nanoantennae *Nano Lett.* **23** 2883–9
[10] Nie S and Emory S R 1997 Probing single molecules and single nanoparticles by surface-enhanced Raman scattering *Science* **275** 1102–6
[11] Cortés E, Etchegoin P G, Le Ru E C, Fainstein A, Vela M E and Salvarezza R C 2010 Monitoring the electrochemistry of single molecules by surface-enhanced Raman spectroscopy *J. Am. Chem. Soc.* **132** 18034–7
[12] Anker J N, Hall W P, Lyandres O, Shah N C, Zhao J and Van Duyne R P 2008 Biosensing with plasmonic nanosensors *Nat. Mater.* **7** 442–53
[13] Langer J *et al* 2020 Present and future of surface-enhanced Raman scattering *ACS Nano* **14** 28–117
[14] Yalavarthi R, Yesilyurt O, Henrotte O, Kment Š and Shalaev V M Boltasseva A and Naldoni A 2022 Multimetallic metasurfaces for enhanced electrocatalytic oxidations in direct alcohol fuel cells *Laser Photon. Rev.* **16** 2200137
[15] Linic S, Christopher P and Ingram D B 2011 Plasmonic-metal nanostructures for efficient conversion of solar to chemical energy *Nat. Mater.* **10** 911–21
[16] Luo S, Mancini A, Wang F, Liu J, Maier S A and De Mello J C 2022 High-throughput fabrication of triangular nanogap arrays for surface-enhanced Raman spectroscopy *ACS Nano* **16** 7438–47
[17] Qi D, Lu L, Wang L and Zhang J 2014 Improved SERS sensitivity on plasmon-free TiO_2 photonic microarray by enhancing light-matter coupling *J. Am. Chem. Soc.* **136** 9886–9
[18] Caldarola M, Albella P, Cortés E, Rahmani M, Roschuk T, Grinblat G, Oulton R F, Bragas A V and Maier S A 2015 Non-plasmonic nanoantennas for surface enhanced spectroscopies with ultra-low heat conversion *Nat. Commun.* **6** 7915
[19] Alessandri I 2013 Enhancing Raman Scattering without plasmons: unprecedented sensitivity achieved by TiO_2 shell-based resonators *J. Am. Chem. Soc.* **135** 5541–4
[20] Fränzl M, Moras S, Gordan O D and Zahn D R T 2018 Interaction of one-dimensional photonic crystals and metal nanoparticle arrays and its application for surface-enhanced Raman spectroscopy *J. Phys. Chem.* C **122** 10153–8
[21] Wang J, Le-The H, Karamanos T, Suryadharma R N S, Van Den Berg A, Pinkse P W H, Rockstuhl C, Shui L, Eijkel J C T and Segerink L I 2020 Plasmonic nanocrystal arrays on photonic crystals with tailored optical resonances *ACS Appl. Mater. Interfaces* **12** 37657–69
[22] Li X, Hu H, Li D, Shen Z, Xiong Q, Li S and Fan H J 2012 Ordered array of gold semishells on TiO_2 spheres: an ultrasensitive and recyclable SERS substrate *ACS Appl. Mater. Interfaces* **4** 2180–5
[23] Wang J, Pinkse P W H, Segerink L I and Eijkel J C T 2021 Bottom-up assembled photonic crystals for structure-enabled label-free sensing *ACS Nano* **15** 9299–327
[24] Mu Z, Gu H, Zhang B, Zheng J, Zhai Z, He X and Zhao Y 2017 FDTD modeling of photonic crystal-incorporated gold nanoparticles for enhancing the localized electric field *J. Mater. Chem.* C **5** 9540–4
[25] Ben-Jaber S, Peveler W J, Quesada-Cabrera R, Cortés E, Sotelo-Vazquez C, Abdul-Karim N, Maier S A and Parkin I P 2016 Photo-induced enhanced Raman spectroscopy for universal ultra-trace detection of explosives, pollutants and biomolecules *Nat. Commun.* **7** 12189
[26] Glass D, Cortés E, Ben-Jaber S, Brick T, Peveler W J, Blackman C S, Howle C R, Quesada-Cabrera R, Parkin I P and Maier S A 2019 Dynamics of photo-induced surface oxygen vacancies in metal-oxide semiconductors studied under ambient conditions *Adv. Sci.* **6** 1901841
[27] Glass D, Quesada-Cabrera R, Bardey S, Promdet P, Sapienza R, Keller V, Maier S A, Caps V, Parkin I P and Cortés E 2021 Probing the role of atomic defects in photocatalytic systems through photoinduced enhanced Raman scattering *ACS Energy Lett.* **6** 4273–81
[28] Liberman V, Yilmaz C, Bloomstein T M, Somu S, Echegoyen Y, Busnaina A, Cann S G, Krohn K E, Marchant M F and Rothschild M 2010 A nanoparticle convective directed assembly process for the fabrication of periodic surface enhanced Raman spectroscopy substrates *Adv. Mater.* **22** 4298–302
[29] Vinnacombe-Willson G A, Conti Y, Stefancu A, Weiss P S, Cortés E and Scarabelli L 2023 Direct bottom-up. *In Situ* growth: a paradigm shift for studies in wet-chemical synthesis of gold nanoparticles *Chem. Rev.* **123** 8488–529
[30] Rambabu Y, Jaiswal M and Roy S C 2015 Enhanced photoelectrochemical performance of multi-leg TiO_2 nanotubes through efficient light harvesting *J. Phys. D: Appl. Phys.* **48** 295302
[31] Rambabu Y, Jaiswal M and Roy S C 2016 Effect of annealing temperature on the phase transition, structural stability and

photo-electrochemical performance of TiO_2 multi-leg nanotubes *Catal. Today* **278** 255–61
[32] Rambabu Y, Dhua S, Jaiswal M and Roy S C 2020 High photoelectrochemical performance of reduced graphene oxide wrapped, CdS functionalized, TiO_2 multi-leg nanotubes *Nanotechnology* **31** 275701
[33] Yalavarthi R *et al* 2021 Enhancing photoelectrochemical energy storage by large-area CdS-coated nickel nanoantenna arrays *ACS Appl. Energy Mater.* **4** 11367–76
[34] Rambabu Y, Kumar U, Singhal N, Kaushal M, Jaiswal M, Jain S L and Roy S C 2019 Photocatalytic reduction of carbon dioxide using graphene oxide wrapped TiO_2 nanotubes *Appl. Surf. Sci.* **485** 48–55
[35] Dutta Roy S, Ghosh M and Chowdhury J 2015 Adsorptive parameters and influence of hot geometries on the SER(R)S spectra of methylene blue molecules adsorbed on gold nanocolloidal particles *J. Raman Spectrosc.* **46** 451–61
[36] Shi X, Ueno K, Oshikiri T, Sun Q, Sasaki K and Misawa H 2018 Enhanced water splitting under modal strong coupling conditions *Nat. Nanotechnol.* **13** 953–8
[37] Le Ru E C, Blackie E, Meyer M and Etchegoin P G 2007 Surface enhanced Raman scattering enhancement factors: a comprehensive study *J. Phys. Chem.* C **111** 13794–803